A Mesoporous Iron−Titanium Oxide Composite Prepared Sonochemically

N. Perkas,[†] O. Palchik,[†] I. Brukental,[‡] I. Nowik,[§] Y. Gofer,[†] Y.Koltypin,[†] and A.Gedanken*,[†]

Department of Chemistry, Bar-Ilan University, Ramat-Gan 52900, Israel, Department of Physics, Bar-Ilan University, Ramat-Gan, 52900, Israel, and Racah Institute of Physics, Hebrew University, Jerusalem 91904, Israel

Received: November 14, 2002; In Final Form: May 28, 2003

Synthesis of a composite mesoporous iron−titanium oxide by ultrasound irradiation is here reported. Iron(III) ethoxide and titanium(IV) isopropoxide were used as precursors, and dodecylamine was used as the templating agent. The synthesis was completed in 6 h in one stage. The product was characterized by XRD, TEM, DSC, TGA, XPS, EDX, and BET methods. Magnetic properties were studied by magnetization and Mössbauer spectroscopy. Short-range ordered structure of the product was demonstrated by low-angle XRD measurements. After heat treatment, this structure collapsed and crystalline phases of γ-Fe_2O_3 oxide and anatase of TiO_2 were observed. The calcinated material showed slight magnetic properties corresponding to the amount of iron oxide. The removal of the surfactant by extraction with diluted nitric acid resulted in the increase of surface area to 650 m^2/g and the pore volume to 0.45 mL/g. The catalytic properties of the material were examined in the oxidation of cyclohexane under mild conditions, and a high conversion of the substrate to cyclohexanol and cyclohexanone was obtained.

I. Introduction

Mesoporous materials play an increasingly important role in different fields of chemical technology, such as electrochemistry, magnetochemistry, and catalysis. The high surface area, large pore volume, and regular pore structure make them very attractive for the design of new effective catalysts with increased activity, selectivity, and stability.[1−6] The ordered mesopores, together with functionalized groups, have been of great use as supports for the active catalytic phases of metal oxides or organometallic compounds.[2,5−10]

The well-known method of preparation of mesoporous nanostructures is based on a liquid crystal templating mechanism. This original synthetic process takes a long time (several days) and is a multiple-step procedure.[11] Ultrasound irradiation has been widely employed in the synthesis of various materials. The sonochemical effect of acoustic cavitation as a continuous formation, growth, and explosive collapse of bubbles within a liquid results in a drastic shortening in the interval of chemical transformations.[12,13] Recently this method has been extended to the preparation of various mesoporous oxides such as mesoporous silica,[14] mesoporous titania,[15] mesoporous yttria−zirconia,[16] and mesoporous iron oxide.[17] The specific advantages in using the sonochemical technique for the synthesis of mesoporous materials are the reduction of time involved in the process from days to hours and the increase of pore wall thickness in the products.[14] We have also reported on the insertion of the active phase of amorphous iron oxide into mesoporous titania by the sonochemical method.[18] The deposited Fe_2O_3 nanoparticles demonstrated a higher activity in a liquid-phase cyclohexane oxidation than nonsupported nanostructured iron oxide or Fe_2O_3 supported on commercial titania.[19] The most effective catalyst for the cyclohexane oxidation was sonochemically prepared mesoporous iron oxide.[17] The increase of catalytic activity of iron(III) inserted in the mesoporous material (MCM-48) was also observed in phenol hydroxylation.[10] In this manuscript we report on our attempt to synthesize a composite mesoporous material based on an iron oxide−titania skeleton by a one-stage sonication process.

It previously has been shown[20−22] that a synergetic effect could be obtained in the oxidation of organic compounds by using catalysts prepared by the coprecipitation of metal oxides. The synthesis of mesoporous composites has also been reported in the literature,[23−25] but the application of composite mesoporous materials in catalysis has not been reported.

II. Experimental Section

The mesoporous iron oxide−titania was prepared from the ethanol solution of iron and titania alkoxides [iron ethoxide (Alfa Aesar) and titanium isopropoxide (Aldrich)] using dodecylamine as a templating surfactant. The molar ratio of $Fe(OEt)_3$ and $Ti(i\text{-}OPr)_4$ was 1:10 or 1:5. The procedure was as follows: 2.5 mmol of $Ti(i\text{-}OPr)_4$ was dissolved in 10 mL of ethanol and 0.8 mmol of dodecylamine was added and marked as a solution (I); 0.25 or 0.50 mmol of $Fe(OEt)_3$ was dissolved in 20 mL of ethanol and labeled solution (II). Both of these solutions were mixed together with a magnetic stirrer for 30 min, added to 140 mL of distilled water in a sonication flask, and a pale precipitate was formed. The flask was filled with water to a volume of 220 mL and sonicated at ambient temperature under air for 5 h (Ti horn, 20 kHz, 70 W/cm^2 at 60% efficiency). The product was separated by centrifugation, was dried under vacuum overnight, and was termed an "as-prepared sample". The surfactant was removed from the pores of the as-prepared precipitate by heating in air or by extraction with a diluted solution of HNO_3 (0.5 M) in ethanol.

The physicochemical properties of the as-prepared and treated samples were characterized by various methods. Elemental

* Author to whom correspondence should be addressed. E-mail: gedanken@mail.biu.ac.il
[†] Department of Chemistry, Bar-Ilan University.
[‡] Department of Physics, Bar-Ilan University.
[§] Racah Institute of Physics, Hebrew University.

10.1021/jp022447v CCC: $25.00
Published on Web 08/05/2003

TABLE 1: Physicochemical Properties of Iron−Titanium Composite Prepared by Ultrasound Irradiation

molar ratio of the reagents $Fe(OEt)_3$:$Ti(i\text{-}OPr)_4$	sample treatment	Fe content, mass %		surface area, m^2/g	pore volume mL/g
		EDX	AAS		
1:10	as prepared	4.6	4.2	237	0.11
	extracted	4.2	3.9	651	0.45
	calcined at 350 °C	5.0	5.5	405	0.21
	calcined at 500 °C	5.3	5.8	150	0.18
1:5	as prepared	8.5	8.8	230	0.10
	extracted	7.4	7.0	462	0.35
	calcined at 350 °C	9.0	9.5	189	0.20
	calcined at 500 °C	9.2	9.7	120	0.16

analysis was carried out by energy dispersed X-ray analysis (EDX) on Link-ISIS-Oxford spectrometer. The iron content was also determined by atomic adsorption spectroscopy (AAS) using a Perkin-Elmer 2380 spectrometer. The phase structure and low-angle (2−10°) X-ray powder diffraction (XRD) patterns were obtained using a Bruker D8 diffractometer with Cu Kα radiation. Transmission electron microscopy (TEM) studies were carried out on JEOL-JEM 100 microscope. The DSC and TGA measurements were made on a Mettler DSC 25 and TGA/STDA 851. The surface area was measured using a Micromeritics (Gemini 2375) analyzer. The nitrogen adsorption and desorption isotherms were obtained at 77 K after heating the sample at 120 °C for 1 h. The surface area was calculated from the linear part of the BET plot. Pore size distribution was estimated using the Barret-Joyner-Halenda (BJH) model with the Halsey equation.[26] The pore volume was measured at the $P/P_o = 0.9947$ signal point. The X-ray photoelectron spectroscopy (XPS) was fulfilled using a KRATOS AXIS HS spectrometer (monochromatic Al Kα). The XPS was studied to evaluate the interaction between the components of the composite mesoporous product. The magnetic measurements were carried out on a Vibrating Sample Magnetometer (VSM-Oxford 3001). The Mössbauer studies were performed using a ^{57}Co:Rh 50 mCi source and a conventional constant acceleration drive Mössbauer spectrometer.

The cyclohexane oxidation reaction was carried out in a thermostated glass reactor using 2 mL (18.5 mmol) of cyclohexane, 2.5 mL (27.75 mmol) of isobutyraldehyde (molar ratio 1.5:1), catalytic amount of acetic acid − 0.06 mL (1 mmol) and 0.1 g of the catalyst. All reagents and solvents used were of analytical grade (Aldrich). The cyclohexane was purified over calcium hydride before the reaction. The reaction mixture was magnetically stirred at 70 °C at 1 atm of oxygen for 15 h. The reaction products were analyzed by GC on a Varian 400, equipped with a packed column (10% Carbowax 400 on Chromosorb 101). Conversion was defined as a percentage of cyclohexane converted into products.

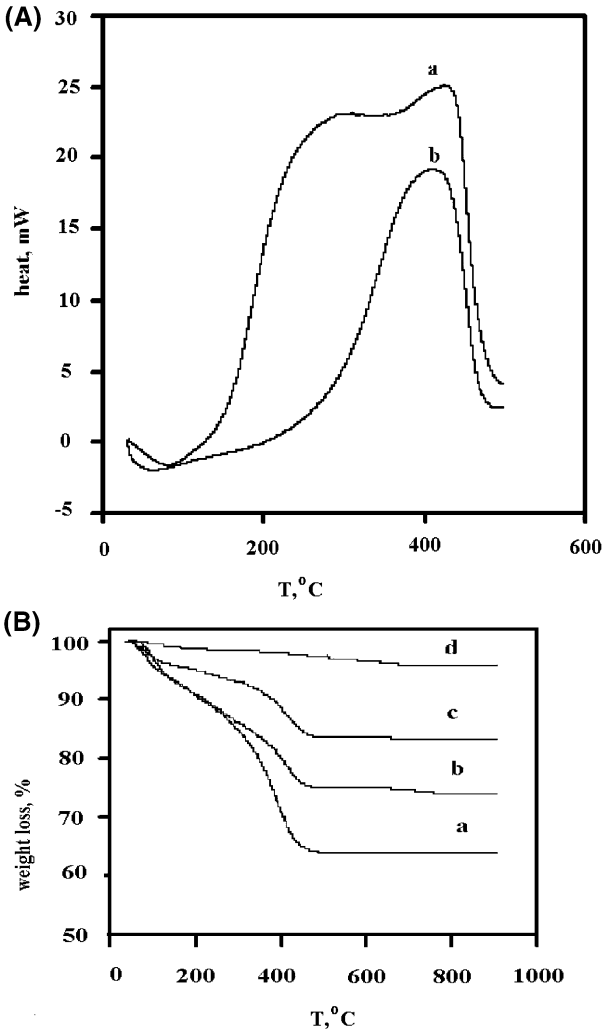

Figure 1. (A) DSC curves of (a) as-prepared material, and (b) after calcination at 500 °C. (B) TGA curves of (a) as-prepared material, (b) after extraction, (c) after calcination at 350 °C, (d) after calcination at 500 °C.

II. Results and Discussion

The results of chemical analysis of the products by EDX and AAS represented in Table 1 are in a good agreement. According to the initial composition of reagents in the reaction solution with the molar ratio of $Fe(OEt)_3$ and $Ti(i\text{-}OPr)_4$ 1:10 and 1:5, the calculated content of iron in the products should be 6.4 and 11.7 mass %, respectively. This means that about 70% of the calculated amount of iron was inserted into the product. The sample prepared with a 1:10 molar ratio of reagents formed a real solution when the alkoxides of Ti and Fe were mixed. On the other hand, when the molar ratio of reagents was 1:5, we obtained a suspension because of the low solubility of iron ethoxide in ethanol. After the extraction process, the sample with the initial molar ratio of 1:5 showed a larger loss of iron due to dissolution in nitric acid. We conclude from these results that only a part of the iron from the original solution was bound to the composite material, and the rest was washed by the solvent. That's why in this manuscript we present only the physicochemical data obtained for the sample prepared with the 1:10 molar ratio of reactants. The removal of the surfactant by heating was accomplished by a slight increase of iron concentration owing to evaporation of the surfactant without loss of iron.

The surfactant removal was followed by DSC and TGA measurements. The DSC patterns of as-prepared sample from 250 to 450 °C showed a broad exothermic peak corresponding to the crystallization of amorphous titania. In fact, a slight saddle was observed at 350 °C (Figure 1A) allowing the broad exothermic peak to be resolved into two peaks. During the second heating cycle, only a slow straight rising line was found

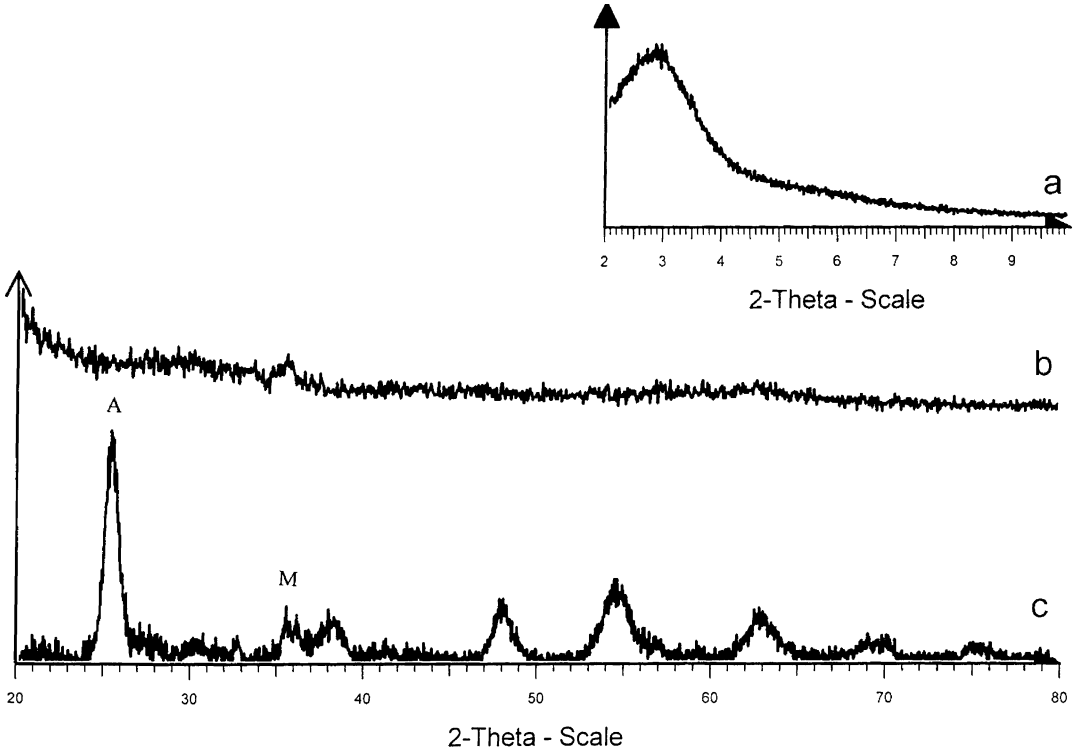

Figure 2. X-ray diffraction patterns for (a) as-prepared material (low angles), (b) after calcination at 350 °C, and after calcination at 500 °C (wide angles); A: anatase; M: maghemite.

and no peaks were observed after 450 °C. This form could be due to the superposition of a stronger exothermic and a weaker endothermic peak. The endothermic peak was attributed to removal of the surfactant, as it was also detected for mesoporous titania prepared previously by the sonication method.[27] For the sample calcined at 500 °C, only one exothermal peak was observed, corresponding to the crystallization of TiO_2. The appearance of an exothermic peak (which has disappeared in the second cycle) in the calcined sample was surprising. The sample was therefore calcined at 600 °C for 3 h and its DSC was scanned. It did not reveal the exothermic peak. According to our interpretation, a complete crystallization of the composite was not achieved when the sample is heated at 500 °C. That is the reason that for such a calcined sample an exothermic peak was detected. On the other hand, when heated at 600 °C the sample was fully crystallized, and the exothermic peak was not observed in the DSC spectrum. These results are in a good agreement with the TGA data. According to the TGA the weight loss took place in steps with a total loss of 25% up to 450 °C (Figure 1B). Above this temperature, no weight loss was observed up to 900 °C. The weight loss for the as- prepared and extracted samples was attributed to the loss of absorbed solvent and surfactant. For the sample heated at 350 °C, only one step of the weight loss was observed corresponding to the removal of the residual of the surfactant. The complete removal of the surfactant was confirmed by the TGA curve of the sample calcined at 500 °C. The weight loss for this sample was negligibly small.

The products were also characterized by X-ray analysis. In the low-angle (2−10°) XRD spectra of the as-prepared product, a broad peak was detected (Figure 2) indicating a short-range ordered structure. This broad feature was interpreted as due to the wormhole-like framework structure similar to what was previously observed for mesoporous titania.[15,27] After heating of the as-prepared product, this peak disappeared because of a deformation of the slightly organized structure.

As expected, the wide-angle XRD spectra of the as-prepared and extracted samples did not show any peaks because of their amorphous nature. After heating 3h at 350 °C under Ar a wide peak appeared that could be referred to γ-Fe_2O_3 (maghemite) (Figure 2). In the sample calcined at 500 °C, the phase crystallinity increased, and there were two additional peaks corresponding to the anatase phase of titania. Annealing of the sample at 500 °C affected also the maghemite peak, which became sharper and more distinct. The maghemite phase was also observed in the mesoporous iron oxide prepared from iron ethoxide.[17] It is worth comparing the current work with our previous work where mesoporous titania was treated with $Fe(CO)_5$ under air for the insertion of iron oxide into the mesopores.[18] When the iron oxide inserted into mesoporous titania was heated in argon, magnetite (Fe_3O_4) and not maghemite (γ-Fe_2O_3) was obtained. The crystallization of magnetite and anatase in that case took place at the same temperature (about 500 °C).[18] In contrast, in the current study, the DSC and XRD measurements showed that the crystallization of iron oxide began at a lower temperature (350 °C) than that of titania (400 °C).

The as-prepared and calcined samples were also characterized by XPS analysis (Figure 3). The binding energy of Ti $2P_{3/2}$ in the as-prepared sample (457.0 eV) was lower than for the heated sample (458.3 eV). The latter corresponds well with the handbook data for titania (458.0 eV). The deconvolution of XPS spectra of as-prepared sample revealed an additional peak that might be associated with the formation of an intermediate compound of TiO_2 which did not appear previously in the XPS of as-prepared mesoporous titania. The lowering of the Ti $2P_{3/2}$ level binding energy may be due to the formation of a Ti−O−Fe bond in the composite mesoporous product. After heating of the as-prepared product, the additional peak in the Ti spectra disappeared as a result of crystallization of the two different phases of maghemite and anatase. Nevertheless, the possibility of such an interaction between Ti and Fe could

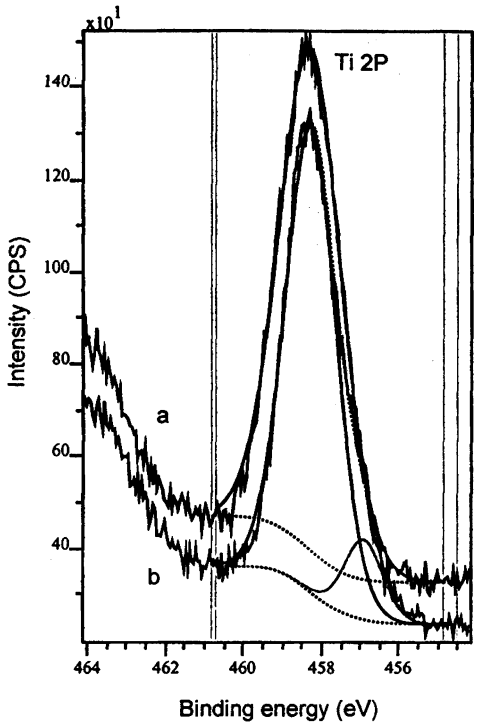

Figure 3. XPS-spectra for (a) as-prepared material, and (b) after calcination at 350 °C.

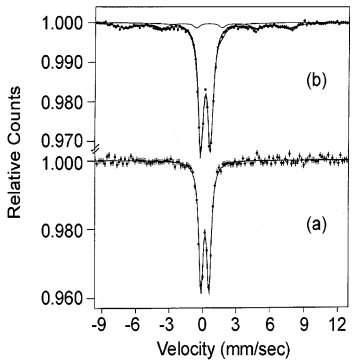

Figure 4. Mössbauer spectra at room temperature for (a) as-prepared material, (b) after calcination at 350 °C.

explain the increase in surface area stability of the synthesized material (Table 1). As for iron oxide, its binding energy was characteristic of the energy level of Fe $2P_{3/2}$, and it did not change very much for as-prepared and heated samples. The peak was found at 711.3 and 710.8 eV for as-prepared and heated samples correspondingly. These energies do not differ very much from the handbook data for Fe_2O_3 (710.9 eV). Perhaps as a result of the low concentration of Fe, these interactions are below the detection limit.

The Mössbauer studies exhibited a pure paramagnetic quadrupole doublet spectrum for the as-prepared sample (Figure 4a). The heated sample demonstrated, in addition to a paramagnetic doublet, also a magnetic sextet (Figure 4b) of a shape typical to a size distribution of superparamagnetic particles. The analysis of the hyperfine interaction parameters of this sextet (isomer shift, 0.4 mm/s, quadrupole interaction, $eqQ/4 = -0.11$ mm/s, and smeared magnetic hyperfine field, average 450 kOe) all indicated that these were Fe_2O_3 particles. These results agreed well with those of the magnetization measurements.

The magnetization measurements of the as-prepared and extracted sample demonstrated a paramagnetic behavior (Figure 5). For the calcined sample the magnetization curves showed a

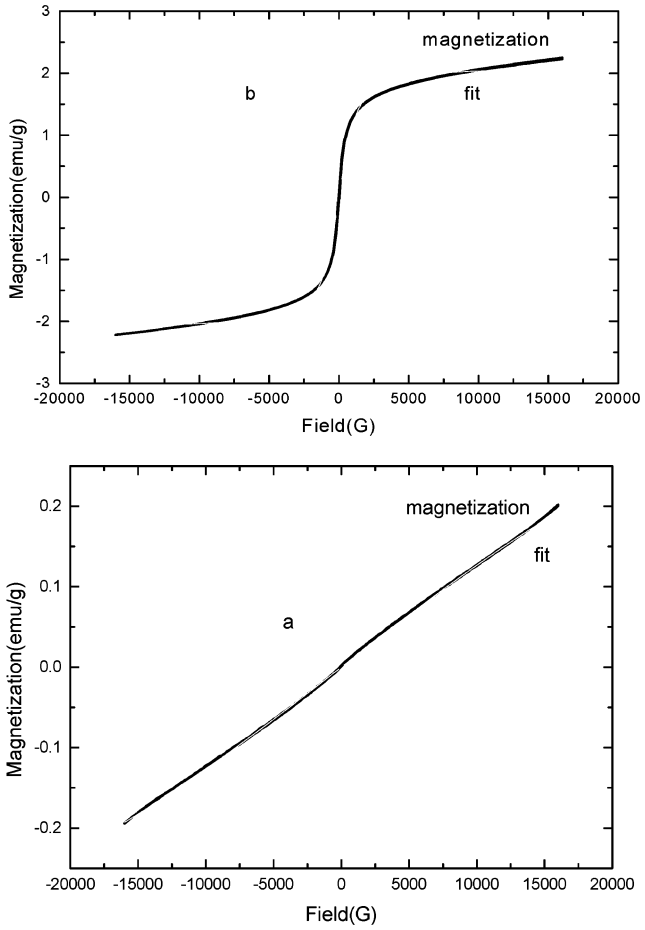

Figure 5. Magnetization curves for (a) as-prepared material, (b) after calcination at 350 °C.

superparamagnetic behavior with remnant magnetization of about 2.0 emu/g. These data confirmed the presence of a magnetic species in the annealed sample which following the XRD and Mossbauer results is assigned to γ-Fe_2O_3 (maghemite). The same magnetic properties were detected in mesoporous iron oxide prepared in our laboratory from iron ethoxide.[17]

The fit for these magnetization curves was according to the Langevin equation

$$\frac{M}{M_0} = \coth\left(\frac{\mu H}{K_B T}\right) - \frac{K_B T}{\mu H}$$

where M is the magnetization per gram, and M_0 is the saturation magnetization, coth is the hyperbolic cotangent, μ is the magnetization per domain, H is the external field, T is temperature, and K_B is the Boltzmann constant. According to this fit, the domain diameter corresponded to about 50 nm in the calcinated sample and about 30 nm in the as-prepared sample. The TEM images revealed that the average particle size in the calcined sample was of 50−100 nm (Figure 6). Good agreement between the TEM and magnetization analysis was obtained for the sizes of the annealed sample. On the other hand, for the as-prepared sample the magnetization analysis yielded particle sizes of 30 nm, while the TEM images showed sizes of 100−200 nm. This discrepancy can be explained as due to the highly agglomerated material that is obtained in the sonication process. The heating process in the first stage helps to deagglomerate the product to its actual particle size (30 nm). This occurs when the solvent molecules, which have glued these

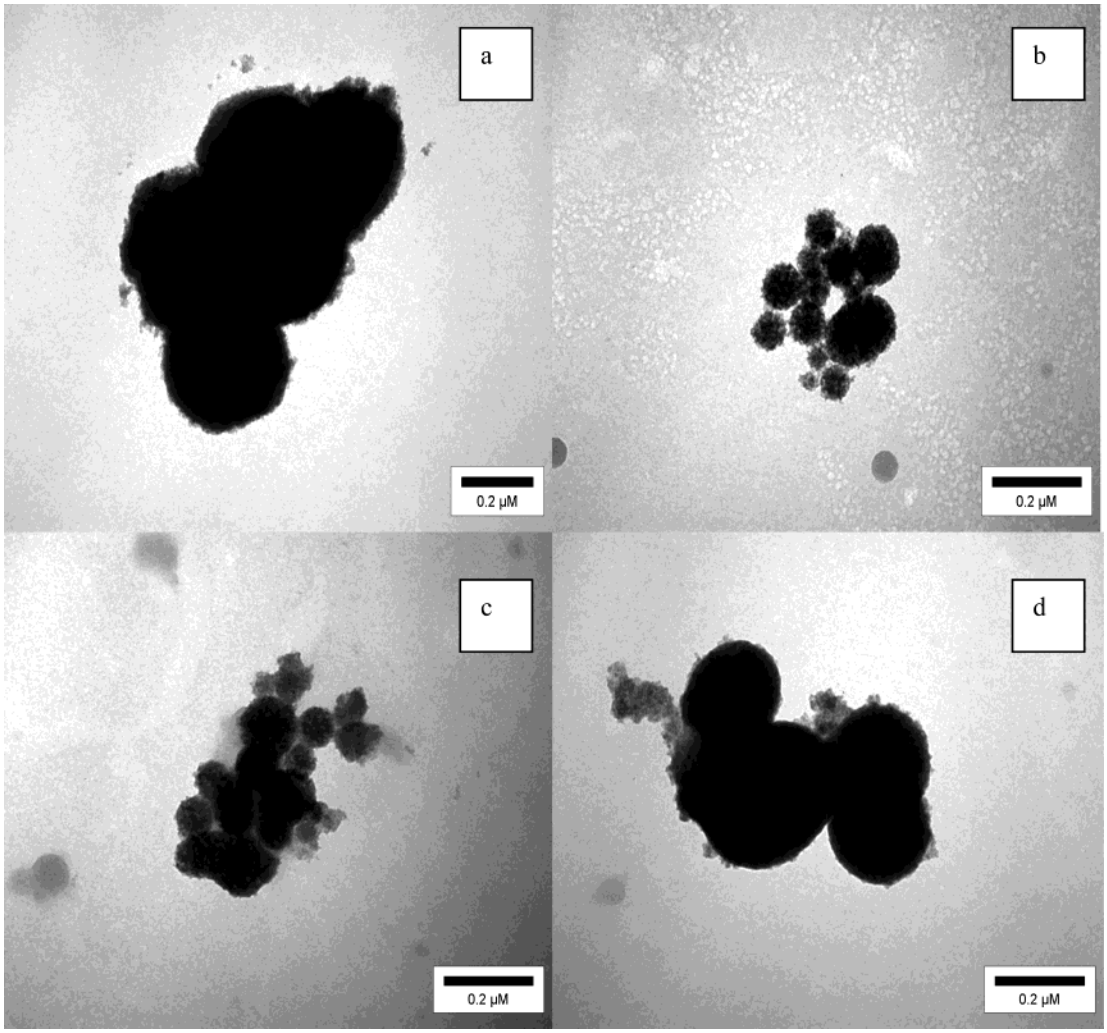

Figure 6. TEM photographs for (a) as-prepared material, (b) after extraction, (c) after calcination at 350 °C, (d) after calcination at 500 °C.

particles together in the aggregates, are evaporated. When the solid is further heated, it sinters and reaches sizes of 50−100 nm.

The TEM micrographs did not reveal any particles of iron oxide as a separate or supported phase, and only a unit structure of the synthesized material was observed.

The TEM images (Figure 6) of as-prepared sample demonstrated relatively large agglomerates, with the size varying from 100 to 200 nm. In the samples extracted and heated at 350 °C, spherical particles of 50 to 100 nm with a pore structure were observed. The space of free pores increased significantly, and the porous structure was more emphasized in that sample in which the surfactant was removed by extraction, rather than when the surfactant was removed by heating at 350 °C. In the sample heated at 500 °C, a growth of the particle size was seen, and was accompanied by a decrease in the surface area. At the same time the spherical form of the particles in the calcinated sample looked more uniform than in the as-prepared material and the porous structure was clear.

These results are in a good agreement with the BET measurements (Table 1). We observed an increase of the surface area and pore volume up to 650 m^2/g and 0.45 mL/g for iron oxide−titania after extraction, and a decrease in these parameters as a result of calcination. For the sample, prepared from the solution of Fe/Ti = 1:10 molar ratio, the surface area and pore volume were higher than for the sample prepared from the suspension of Fe/Ti = 1:5 molar ration. This could be explained by the observation that in the material of Fe/Ti = 1:5 molar ratio, not all the iron ethoxide was dissolved in the ethanol solution and connected to the composite material. As a result, part of the iron oxide was, perhaps, deposited over titanium oxide and blocked the pores, thereby reducing the surface area. It should be noted, that the decrease of surface area for both samples after heating for 3 h at 500 °C was not so drastic as was observed for mesoporous titania without iron oxide (from 700 to 750 to 80 m^2/g).[15] In our case, the surface area after annealing was only 3−4 times lower than after extraction. This could be considered to be a result of specific interaction between iron oxide and titania during their simultaneous precipitation under ultrasound irradiation. This interaction hindered the collapse of the mesoporous structure. The wall thickness of the studied material increased from 4 to 5 Å for pristine TiO_2(MSP) without iron oxide, to 7−8 Å for the composite structure.

In Figure 7 the adsorption−desorption isotherms of samples treated by extraction and calcination at 350 °C and 500 °C are represented. According to the form of the isotherms, they could not be referred to the H4 type isotherms characteristic of regular mesoporous sorbents. Nevertheless, at relatively high-pressure $P/P_o > 0.6$, for samples extracted and heated at 350 °C a hysteresis was observed. According to the BJH model the predominant pore diameter of these samples was about 30 Å, that together with all the other reported results allows them to be considered as the mesoporous materials. On the other hand, the isotherms of the pristine TiO_2(MSP) and that of iron oxide

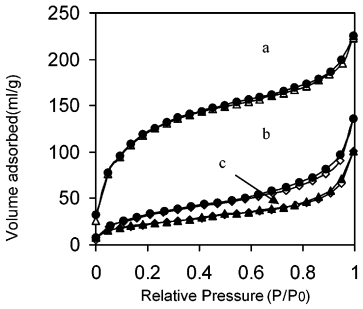

Figure 7. Adsorption−desorption isotherm for (a) extracted material, (b) calcinated at 350 °C, (c) calcinated at 500 °C.

TABLE 2: Oxidation of Cyclohexane Using Highly Dispersed Iron Oxide Catalysts (1 atm O_2, 70 °C)

catalyst	content of Fe_2O_3, mass %	conversion, %	Ol:one[a]
Fe_2O_3(nanostructured)	100	16.5	1.5:1
Fe_2O_3/TiO_2(Degussa)	12.0	21.3	1.1:1
Fe_2O_3/TiO_2(mesoporous)	14.5	25.8	1.5:1
Fe_2O_3(mesoporous)	100	35.8	5:1
Fe_2O_3/TiO_2 composite (1:10)	6.0	30.3	3:1
Fe_2O_3/TiO_2 composite (1:5)	10.6	28.3	3:1

[a] Molar ratio of cyclohexanol to cyclohexanone.

inserted in TiO_2(MSP) did not show hysteresis for the heat-treated (at 350 °C) products.[18,27] This is an indication of the difference in formation and increase of thermal stability of the composite material with mesoporous structure.

The catalytic activity of iron oxide−titania mesoporous composites was studied in the reaction of the cyclohexane oxidation under mild conditions. The activity of the catalysts was mainly caused by the presence of a high-dispersed iron-(III) phase as was also shown previously.[18,19] Without addition of iron, TiO_2(MSP) itself did not catalyze the oxidation process. The mechanism of the reaction has been discussed in our previous publications, and it follows the mechanism suggested by Murahashi.[28] The conversion of cycloalkane with new iron oxide−titania mesoporous catalyst was found to be higher than that with iron oxide nanoparticles inserted into the mesoporous titania. However, the conversion of the initial product was lower than with mesoporous iron oxide as a catalyst (Table 2). It should be mentioned that the concentration of iron oxide in this composite material is lower than in the supported catalysts, and the increase in the catalytic activity has been demonstrated as the synergetic effect of the two oxide phases presented. The catalyst prepared with the molar ratio of the components $Fe(OEt)_3$ and $Ti(i\text{-}OPr)_4$ of 1:5 was less active than that of the composite prepared with the molar ratio 1:10. The former composition, probably, combined the properties of the iron oxide catalyst supported over mesoporous titania and the composite iron−titania catalyst. The selectivity for the target products cyclohexanol and cyclohexanone was close to 90%. This molar ratio of the two main products was higher than the molar ratio obtained with the iron oxide nanoparticles supported over titania. The activity of the catalysts did not change after 3 cycles of oxidation experiments. The most important feature of new composite catalyst was that leaching of iron was not observed in the product of the catalytic reaction, while with the iron oxide supported on titania (Degussa) or inserted into titania mesoporous some leaching of iron into the reaction solution took place. This observation also indicates the strong interaction between iron oxide and titania in the composite material.

IV. Conclusion

Mesoporous iron oxide−titania was prepared by the surfactant templating method using the sonochemical technique. The synthesis was carried out in a one-stage process and lasted 6 h. The results of physicochemical studies indicated the formation of the short-range ordered mesoporous structure. After heating, it crystallized into the γ-Fe_2O_3 and anatase phase of TiO_2. As a result, some magnetic properties corresponding to maghemite's concentration in the product were found. The removal of the surfactant by extraction with dilute nitric acid led to the increase of surface area of the material up to 650 m^2/g, and its high catalytic activity and stability in the oxidation of cyclohexane under mild conditions were demonstrated. The activity of the iron(III) oxide phase, which is responsible for the oxidation reaction, was effected by interaction with titania. Although we could not obtain direct evidence for the interaction of titania and the iron oxide, circumstantial findings such as the specific order of crystallization, the increased thermal stability of the mesoporous structure, the increase of the pore wall thickness, the higher catalytic activity, the increased stability of the active phase of iron oxide toward leaching into the reaction solution, and the formation of additional (Ti-bond) during the synthesis; all indicate the interaction of iron and titania and their integration in the mesoporous composite material.

Acknowledgment. Prof. A. Gedanken thanks the German Ministry of Science through the Deutsche-Israel program, DIP, for its support.

References and Notes

(1) Antonelli, D. M.; Ying, Y. J. *Chem. Mater*. **1996**, *8*, 874.
(2) Sayari, A.; Hamoudi, S. *Chem. Mater*. **2001**, *10*, 13.
(3) Jaroniec, M.; Kruk, M.; Shin, H. J.; Ryoo, R.; Sakamoto, Y.; Terasaki, O. *Microporous Mesoporous Mater*. **2001**, *1*−*3*, 48.
(4) Corma, A. *Chem. Rev*. **1997**, *97*, 3273.
(5) Barton, T. J.; Bull, L. M.; Klemperer, G. *Chem. Mater*. **1999**, *11*, 2633.
(6) Braun, P. V.; Osenar, P.; Tohvev, V.; Kennedy, S. B.; Stupp, S. I. *J. Am. Chem. Soc*. **1999**, *121*, 7302.
(7) Brunel, D.; Canvel, A.; Fajula, F.; Renzo, F. D. *Stud. Surf. Sci. Catal*. **1995**, *97*, 173.
(8) Kozhevnikov, I. V.; Sinnema, A.; Yansen, R. J. J.; Ranin, K.; van Bekkem, H. *Catal. Lett*. **1995**, *30*, 241.
(9) Bleloch, A.; Jonson, B. F. J.; Ley, S. V.; Price, A. J.; Shephard, D. S.; Thomas, A. W. *Chem. Commun*. **1999**, 1907.
(10) Zhao, W.; Yunfei, L.; Peng, D.; Quanzhi, L. *Catal. Lett*. **2001**, *73*, 199.
(11) Kresge, C. T.; Leonowicz, M. E.; Roth, W.; Vartulli, J. C.; Beck J. S. *Nature* **1992**, *359*, 710.
(12) Suslik, K. S.; Choe, S. B.; Cichowlas, A. A.; Grinstaff, M. S. *Nature* **1991**, *353*, 414.
(13) Suslik, K. S.; Hueon, T.; Fang, M.; Cichowlas, A. A. *Mater. Sci. Eng*. A **1995**, *204*, 186.
(14) Tang, X.; Lius, S.; Wang, Y; Huang, W.; Sominski, E.; Palchik, O.; Koltypin, Y.; Gedanken, A. *Chem. Commun*. **2000**, 2119.
(15) Wang, Y.; Tang, X.; Yin, L.; Huang, W.; Rosenfeld Hacohen, Y.; Gedanken A. *Adv. Mater*. **2000**, *12*, 1183.
(16) Wang, Y.; Yin, L.; Palchik, O.; Rosenfeld Hacohen, Y.; Koltypin, Y.; Gedanken, A. *Langmuir* **2001**, *17*, 4131.
(17) Srivastava, D. N.; Perkas, N.; Gedanken, A.; Felner, I. *J. Phys. Chem*. B **2002**, *106*, 1878.
(18) Perkas, N.; Wang, Y.; Koltypin, Y.; Gedanken, A.; Chanderasekaran, S. *Chem. Commun*. **2001**, 988.
(19) Perkas, N.; Koltypin, Y.; Palchik, O.; Gedanken, A.; Chanderasekaran, S. *Appl. Catal., A - Gen*. **2001**, *209*, 125.
(20) Buciuman, F. C.; Patcas, F.; Hahn, T. *Chem. Eng. Proc*. **1999**, *38*, 563.
(21) Hashimoto, K.; Wasado, K.; Osaki, M.; Shono, E.; Adachi, K.; Toukai, N.; Kominami, H.; Kera, Y. *Appl. Catal., B - Environ*. **2001**, *429*, 30.
(22) Chen, H.; Syari, A.; Adnot, A.; Larachi, F. *Appl. Catal. B, Environ*. **2001**, *32*, 195.

(23) Wang, Z.; Lan, T.; Pinnavia, T. J. *Chem. Mater*. **1996**, *8*, 2200.
(24) Fudala, A.; Kiricsi, L.; Niwa, S. I.; Toba, M.; Kiyosumi, Y.; Mizukami, F. *J. Therm. Anal. Calorim*. **1996**, *56*, 227.
(25) Wirnsberger, G.; Gatterer, K.; Fritzer, H. P.; Grogger, W.; Pillep, B.; Behrens, P.; Hansen, M. F.; Hansen, M. F.; Bender Koch, C. *Chem. Mater*. **2001**, *13*, 1467.
(26) Gregg, S. J.; Sing, K. S. Adsorption Surface Area and Porosity; Academic Press: London, 1982.
(27) Wang, Y.; Chen, S.; Tang, X.; Palchik, O.; Zaban, A.; Koltypin, Y.; Gedanken, A. *J. Mater. Chem*. **2001**, *11*, 521.
(28) Murahashi, S. T.; Oda, Y.; Naota, T. *J. Am. Chem. Soc*. **1992**, *114*, 7913.